

Hydrogen Bonding Interfaces in Fullerene•TTF Ensembles

Margarita Segura,[†] Luis Sánchez,[‡] Javier de Mendoza,^{*,†} Nazario Martín,^{*,‡} and Dirk M. Guldi^{*,§}

Contribution from the Departamento de Química Orgánica, Universidad Autónoma de Madrid, Cantoblanco, E-28049, Madrid, Spain, Departamento de Química Orgánica I, Facultad de Química, Universidad Complutense, E-28040 Madrid, Spain, and Radiation Laboratory, University of Notre Dame, Notre Dame, Indiana 46556

Received May 27, 2003; E-mail: javier.demendoza@uam.es; nazmar@quim.ucm.es; guldi.1@nd.edu

Abstract: Novel thermodynamically stable supramolecular donor–acceptor dyads have been synthesized. In particular, we assembled successfully C₆₀, as an electron acceptor, with the strong electron donor TTF through a complementary guanidinium-carboxylate ion pair. Two strong and well-oriented hydrogen bonds, in combination with ionic interactions, ensure the formation of stable donor–acceptor dyads. The molecular architecture has been fine-tuned by using chemical spacers of different lengths (i.e., phenyl versus biphenyl) and functional groups (i.e., ester versus amide), thus providing meaningful incentives to differentiate between through-bond and through-space electron-transfer scenarios. In electrochemical studies, both the donor and acceptor character of the TTF and C₆₀ units, respectively, have been clearly identified. Steady-state and time-resolved emission studies, however, show a solvent-dependent fluorescence quenching in C₆₀•TTF dyads as well as the formation of the C₆₀^{•-}•TTF^{•+} radical ion pairs, for which we determined lifetimes that are in the range of hundred of nanoseconds to microseconds. The complex network that connects C₆₀ with TTF in the dyads and the flexible nature of the spacer result in through-space electron-transfer processes. This first example of electron transfer in C₆₀-based dyads, connected by strong hydrogen bonds, demonstrates that this approach can add outstanding benefits to the construction of artificial photosynthetic systems that bear a closer resemblance to the natural one.

Introduction

Photoinduced energy and electron-transfer processes bear great significance in nature since they govern photosynthesis in plants and bacteria.¹ In the context of engineering extended 1-D, 2-D, or 3-D model systems, meaningful incentives are lent from bacterial photosynthetic reaction centers. In these natural analogues, the required well-defined architectures are often achieved, with high directionality and selectivity, by multipoint interactions between the individual building blocks, including hydrogen bond motifs.²

Owing to the versatility that biomimetic methodologies provide as meaningful organization principles to regulate size, shape, and function down to the nanometer scale, they are widely spread in use for the preparation of simple artificial photosynthetic systems³ or as models for electron-transfer theory.⁴ A central benefit of biomimetic motifs is that they are

reversible, and in contrast to truly covalent bonds, their binding energies are highly dependent on the chemical environment and temperature.

Fullerenes exhibit remarkable physicochemical features, which render them promising building blocks for the integration into functional molecular assemblies and supramolecular arrays.^{5,6} Among several outstanding properties, the spherical shape of fullerenes, giving rise to a delocalized π -electron system, offers unique opportunities for stabilizing charged entities. As a consequence, small reorganization energies are found for C₆₀ in electron-transfer processes, which accelerate the initial charge separation, while the strongly exothermic charge recombination is decelerated, due to being shifted deeply into the “inverted region”. Despite the current interest to incorporate fullerene components into supramolecular systems,⁷ only a few examples have been reported so far, in which hydrogen bonding motifs dictate the structural arrangement⁸ or the transduction of excited-state energy between donors and C₆₀.⁹

In the context of preparing new photovoltaic materials, the integration of C₆₀ and tetrathiafulvalene (TTF)¹⁰ or C₆₀ and exTTF (exTTF, π -conjugated *p*-quinonoid-TTF) into synthetic reaction center models (i.e., covalently linked C₆₀-TTF and C₆₀-

[†] Universidad Autónoma de Madrid.

[‡] Universidad Complutense.

[§] Radiation Laboratory, University of Notre Dame.

- (1) (a) Wasielewski, M. R. *Chem. Rev.* **1992**, *92*, 435–461. (b) Moser, C. C.; Keske, J. M.; Warncke, K.; Farid, R. S.; Dutton, P. L. *Nature* **1992**, *355*, 796–802. (c) Regan, J. J.; Onuchic, J. N. In *The Reaction Centers of Photosynthetic Bacteria*; Michel-Beyerle, M. E., Ed.; Springer: Berlin, 1996.
- (2) (a) Lehn, J.-M. *Supramolecular Chemistry*; VCH: Weinheim, 1995. (b) Steed, J. W.; Atwood, J. L. *Supramolecular Chemistry*; Wiley: Chichester, 2000. (c) Sherrington, D. C.; Taskinen, K. A. *Chem. Soc. Rev.* **2001**, *30*, 83–93.
- (3) Ward, M. D. *Chem. Soc. Rev.* **1997**, *26*, 365–375.
- (4) Marcus, R. A. *Pure Appl. Chem.* **1997**, *69*, 13–29.

(5) For a recent review, see: Guldi, D. M.; Martín, N. *J. Mater. Chem.* **2002**, *12*, 1978–1992.

(6) Special issue on Functionalized Fullerene Materials, Prato, M.; Martín, N., Eds. *J. Mater. Chem.* **2002**, *12*, 1931–2159.

(7) Diederich, F.; Gómez-López, M. *Chem. Soc. Rev.* **1999**, *28*, 263–277.

exTTF)¹¹ emerged as a particularly promising approach.^{12,13} Typically, photoexcitation of these C₆₀-TTF and C₆₀-exTTF systems leads to highly energetic and long-lived charge separated states. The charge-separation lifetimes vary from a few nanoseconds to hundreds of microseconds and can be controlled at will: Important variables in control over the lifetimes are solvent environment, donor–acceptor separation, electronic coupling element, and so forth. Since a significant fraction of the photon energy (up to 80%) is converted and stored in the form of charge-separated states (~1.1–1.5 eV), it permits the possibility to minimize the loss of excited-state energy and, thereby, to improve the conversion efficiency of solar energy into electrical and chemical energy.

In the current work, we wish to report on the synthesis of several new C₆₀•TTF ensembles, in which a photoexcited-state acceptor (C₆₀) and an electroactive donor (TTF) are held together through hydrogen bonding interactions that are based on the complementary guanidinium and carboxylate motifs.¹⁴ To add structural diversity to the C₆₀•TTF ensembles, two different functionalities, namely, ester or amide groups, have been

employed in connecting C₆₀ and TTF to the guanidinium and carboxylate moieties in several protocols. As a result, we isolated a series of topologically different H-bonding dyads whose physicochemical properties have been examined by cyclic voltammetry, fluorescence spectroscopy, and transient absorption spectroscopy. From the spectroscopic characterization, we conclude the formation of charge-separated radical pairs, C₆₀•⁻TTF^{•+}, that exhibit lifetimes in the range of hundreds of nanoseconds, evolving from photoinduced electron-transfer processes that occur, in large, via through-space interactions.

Results and Discussion

In the present study, we probed the assembly of the strong electron acceptor C₆₀ with the strong electron donor TTF, through a guanidinium-carboxylate ion pair involving two strong and well-oriented donor–donor–acceptor–acceptor (DD-AA) hydrogen bonds in combination with an electrostatic interaction, toward thermodynamically stable supramolecular donor–acceptor dyads. An important aspect of our work is the fine-tuning of the molecular architecture, which was accomplished by using spacers of different lengths and of different hydrogen bond orientations (donors, **1a,b** and **4**; acceptors, **2a,b**, **3a,b**, **5**, and **6**; see Chart 1).

A closer inspection of the guanidinium/donor or acceptor connection reveals some structural flexibility, and different structural conformers are assumed to be present in the resulting ensembles (Chart 2).

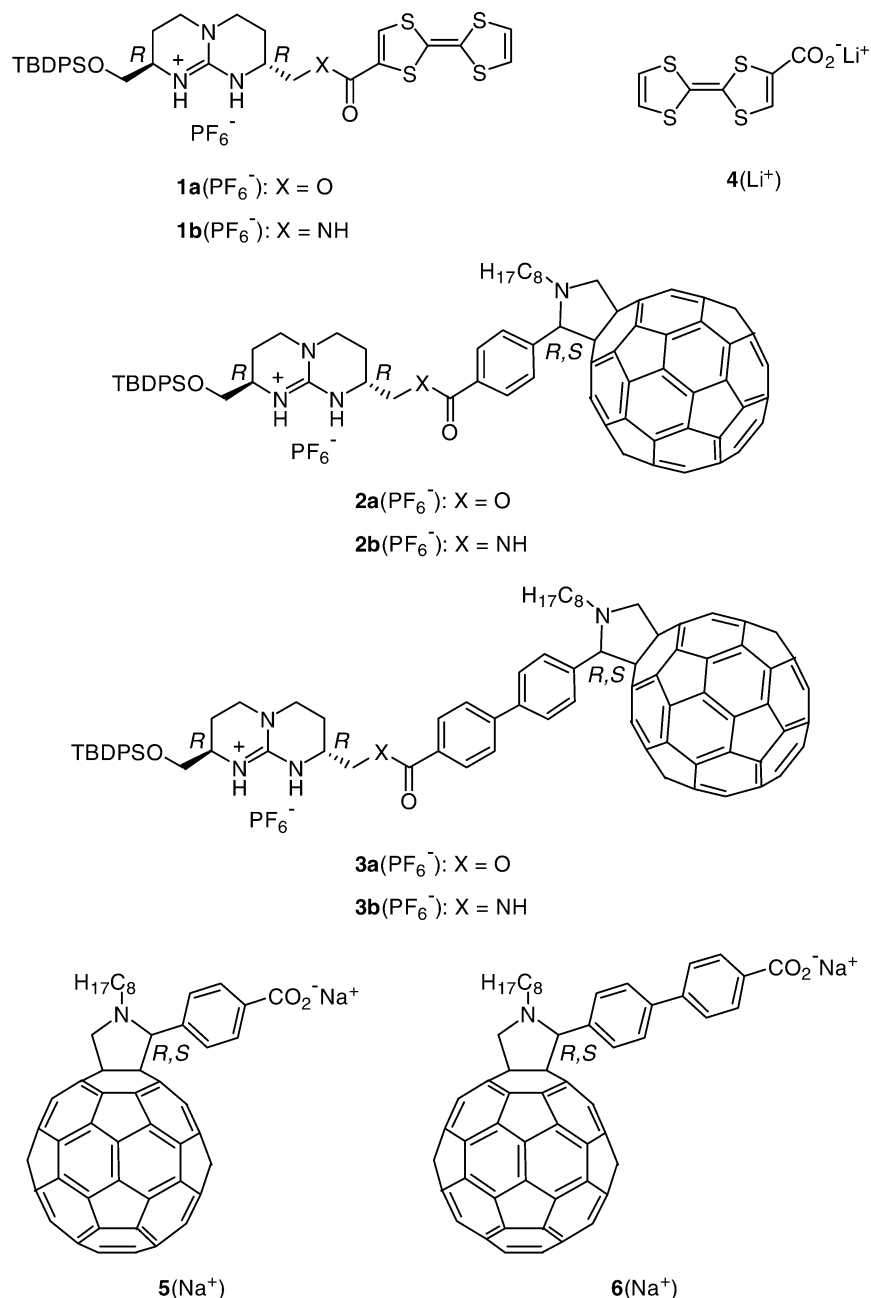
Charge-transfer interactions, as they may well prevail between the donor (TTF) and acceptor (C₆₀), impose, on the other hand, a certain degree of control over orientation and structure. To constitute a useful way for elucidating such structural conformations, we pursued the use of oppositely oriented hydrogen bond motifs (see for illustration dyads **1a•5** and **2a•4**) which should result in different electron-transfer responses.

Synthesis. The synthesis of guanidinium-TTF derivatives **1a,b** is summarized in Scheme 1. Both compounds were prepared in moderate (49%) and good yields (72%), respectively, from acyl chloride **10**¹⁵ via coupling with the appropriate guanidinium salt [alcohol **7**(PF₆⁻) or amine **9**].¹⁶ The use of reverse-phase silica gel chromatography for the purification of ester **1a**(PF₆⁻) is central, since it prevented hydrolysis of this otherwise relatively unstable derivative.

The phenyl-C₆₀ derivatives (Scheme 2) were obtained by PyBOP (benzotriazole-1-yl-oxytripyrrolidinophosphonium hexafluorophosphate) activation of carboxylic acid **12**, which was synthesized from *p*-formylbenzoic acid (**11**), C₆₀, and *N*-octylglycine in 52% yield.¹⁷ In a succeeding reaction with the chiral guanidinium salt [**7**(Cl⁻) or **9**], **2a,b** were isolated as hexafluorophosphate salts with good yields.

In a similar way, biphenyl-C₆₀ compounds **3a,b** were prepared from acid **15**. The latter was synthesized in racemic form by reacting 4'-formylbiphenyl-4-carboxylic acid methyl ester (**13**)¹⁸

- (8) (a) Diederich, F.; Echegoyen, L.; Gómez-López, M.; Kessinger, R.; Stoddart, J. F. *J. Chem. Soc., Perkin Trans. 2* **1999**, 1577–1586. (b) Rispens, M. T.; Sánchez, L.; Knol, J.; Hummelen, J. C. *Chem. Commun.* **2001**, 161–162. (c) González, J. J.; González, S.; Priego, E. M.; Luo, C. P.; Guldi, D. M.; de Mendoza, J.; Martín, N. *Chem. Commun.* **2001**, 163–164. (d) Sánchez, L.; Rispens, M. T.; Hummelen, J. C. *Angew. Chem., Int. Ed.* **2002**, *41*, 838–840. (e) Beckers, E. H. A.; Schenning, A. P. H. J.; van Hal, P. A.; El-ghayoury, A.; Sánchez, L.; Hummelen, J. C.; Meijer, E. W.; Janssen, R. A. J. *Chem. Commun.* **2002**, 2888–2889.
- (9) (a) Beckers, E. H. A.; van Hal, P. A.; Schenning, A. P. H. J.; El-ghayoury, A.; Peeters, E.; Rispens, M. T.; Hummelen, J. C.; Meijer, E. W.; Janssen, R. A. J. *J. Mater. Chem.* **2002**, *12*, 2054–2060. (b) Guldi, D. M.; Ramey, J.; Martínez-Díaz, M. V.; de la Escosura, A.; Torres, T.; Da Ros, T.; Prato, M. *Chem. Commun.* **2002**, 2774–2775. (c) Guldi, D. M.; Gouloumis, A.; Vázquez, P.; Torres, T. *Chem. Commun.* **2002**, 2056–2057.
- (10) For a review on recent applications of TTF, see: Segura, J. L.; Martín, N. *Angew. Chem., Int. Ed.* **2001**, *40*, 1372–1409.
- (11) (a) Martín, N.; Ortí, E. In *Handbook of Advanced Electronic and Photonic Materials and Devices*; Nalwa, H. S., Ed.; Academic Press: New York, 2001; Vol. 3, Chapter 6. (b) Yamashita, Y.; Kobayashi, Y.; Miyashita, T. *Angew. Chem., Int. Ed. Engl.* **1989**, *28*, 1052–1055. (c) Bryce, M. R.; Moore, A. J.; Hasan, M.; Ashwell, G. J.; Fraser, A. T.; Clegg, W.; Hursthouse, M. B.; Karaulov, A. I. *Angew. Chem., Int. Ed. Engl.* **1990**, *29*, 1450–1452.
- (12) (a) Guldi, D. M.; González, S.; Martín, N.; Antón, A.; Garín, J.; Orduna, J. *J. Org. Chem.* **2000**, *65*, 1978–1983. (b) Martín, N.; Sánchez, L.; Herranz, M. A.; Guldi, D. M. *J. Phys. Chem. A* **2000**, *104*, 4648–4657. (c) Martín, N.; Sánchez, L.; Guldi, D. M. *Chem. Commun.* **2000**, 113–114. (d) Segura, J. L.; Priego, E. M.; Martín, N.; Luo, C. P.; Guldi, D. M. *Org. Lett.* **2000**, *2*, 4021–4024. (e) Herranz, M. A.; Martín, N.; Ramey, J.; Guldi, D. M. *Chem. Commun.* **2002**, 2968–2969. (f) González, S.; Martín, N.; Guldi, D. M. *J. Org. Chem.* **2003**, *68*, 779–791. (g) González, S.; Martín, N.; Swartz, A.; Guldi, D. M. *Org. Lett.* **2003**, *5*, 557–560. (h) Sánchez, L.; Pérez, I.; Martín, N.; Guldi, D. M. *Chem. Eur. J.* **2003**, *9*, 2457–2468.
- (13) (a) Liddell, P. A.; Kodis, G.; de la Garza, L.; Bahr, J. L.; Moore, A. L.; Moore, T. A.; Gust, D. *Helv. Chim. Acta* **2001**, *84*, 2765–2783. (b) Kreher, D.; Cariou, M.; Liu, S.-G.; Levillain, E.; Veciana, J.; Rovira, C.; Gorgues, A.; Hudhomme, P. *J. Mater. Chem.* **2002**, *12*, 2137–2159 and references therein. (c) Kodis, G.; Liddell, P. A.; de la Garza, L.; Moore, A. L.; Moore, T. A.; Gust, D. *J. Mater. Chem.* **2002**, *12*, 2100–2108.
- (14) (a) Müller, G.; Riede, J.; Schmidtchen, F. P. *Angew. Chem., Int. Ed. Engl.* **1988**, *27*, 1516–1518. (b) Echavarren, A.; Galán, A.; Lehn, J.-M.; de Mendoza, J. *J. Am. Chem. Soc.* **1989**, *111*, 4994–4995. (c) Gleich, A.; Schmidtchen, F. P.; Mikulcik, P.; Müller, G. *J. Chem. Soc., Chem. Commun.* **1990**, 55–58. (d) Schiess, P.; Schmidtchen, F. P. *Tetrahedron Lett.* **1993**, *34*, 2449–2452. (e) Fan, E.; van Arman, S. A.; Kincaid, S.; Hamilton, A. D. *J. Am. Chem. Soc.* **1993**, *115*, 369–370. (f) Chicharro, J.-L.; Prados, P.; de Mendoza, J. *J. Chem. Soc., Chem. Commun.* **1994**, 1193–1194. (g) Albert, J. S.; Goodman, M. S.; Hamilton, A. D. *J. Am. Chem. Soc.* **1995**, *117*, 1143–1144. (h) Seel, C.; Galán, A.; de Mendoza, J. *Top. Curr. Chem.* **1995**, *175*, 101–132. (i) Segura, M.; Alcázar, V.; Prados, P.; de Mendoza, J. *Tetrahedron* **1997**, *53*, 13119–13128. (j) Pecuh, M. W.; Hamilton, A. D.; Sánchez-Quesada, J.; de Mendoza, J.; Haack, T.; Giralt, E. *J. Am. Chem. Soc.* **1997**, *119*, 9327–9328. (k) Haack, T.; Pecuh, M. W.; Salvatella, X.; Sánchez-Quesada, J.; de Mendoza, J.; Hamilton, A. D.; Giralt, E. *J. Am. Chem. Soc.* **1999**, *121*, 11813–11820. (l) Salvatella, X.; Pecuh, M. W.; Gairi, M.; Jain, R. K.; Sánchez-Quesada, J.; de Mendoza, J.; Hamilton, A. D.; Giralt, E. *Chem. Commun.* **2000**, 1399–1400. (m) Orner, B. P.; Salvatella, X.; Sánchez-Quesada, J.; de Mendoza, J.; Giralt, E.; Hamilton, A. D. *Angew. Chem., Int. Ed.* **2002**, *41*, 117–119.
- (15) Panetta, C. A.; Baghdadchi, J.; Metzger, R. M. *Mol. Cryst. Liq. Cryst.* **1984**, *107*, 103–113.
- (16) Breccia, P.; Van Gool, M.; Pérez-Fernández, R.; Martín-Santamaría, S.; Gago, F.; Prados, P.; de Mendoza, J. *J. Am. Chem. Soc.* **2003**, *125*, 8270–8284.
- (17) For a general approach to the synthesis of fulleropyrrolidines, see: (a) Maggini, M.; Scorrano, G.; Prato, M. *J. Am. Chem. Soc.* **1993**, *115*, 9798–9799. (b) Prato, M.; Maggini, M. *Acc. Chem. Res.* **1998**, *31*, 519–526. (c) Tagmatarchis, N.; Prato, M. *Synlett* **2003**, *6*, 768–779.
- (18) Blettner, C. G.; König, W. A.; Stenzel, W.; Schotten, T. *J. Org. Chem.* **1999**, *64*, 3885–3890.

Chart 1. Structures of Guanidinium Compounds **1–3a,b** and Carboxylates **4–6**

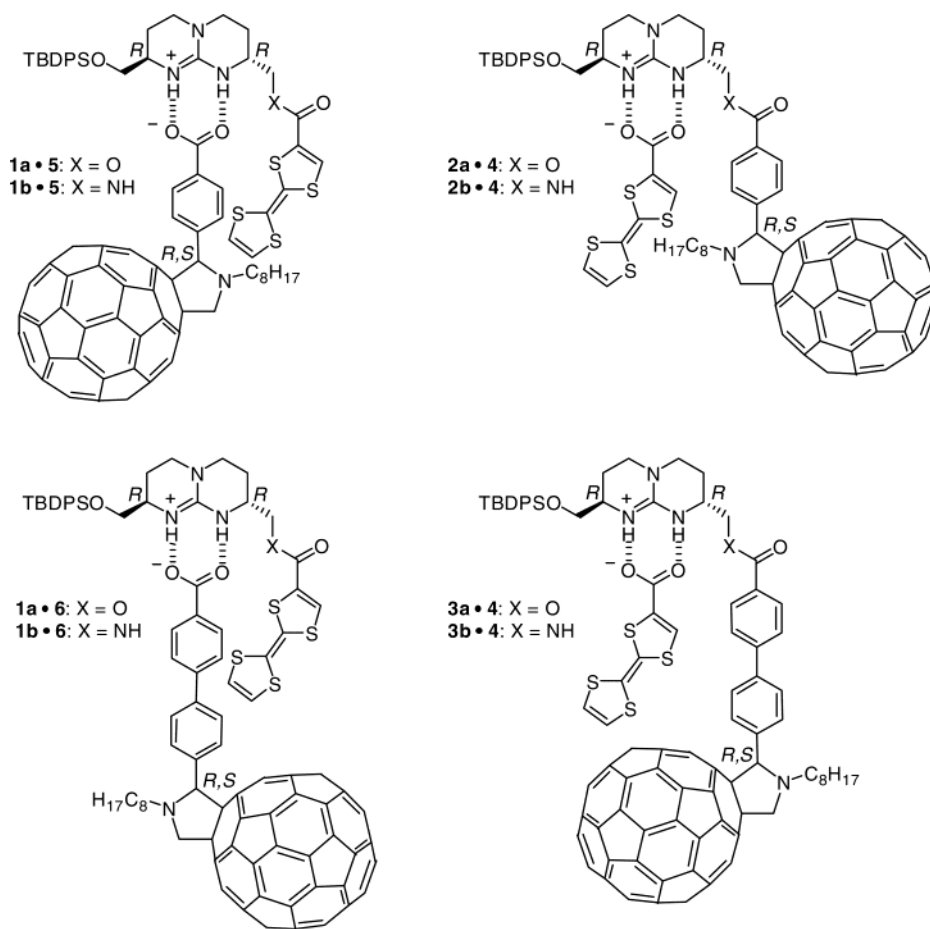
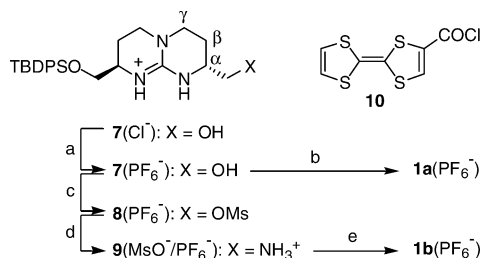
with C₆₀ and *N*-octylglycine and subsequently deprotected in an acidic medium (Scheme 3).

All new compounds were fully characterized by a variety of spectroscopic and spectrometric techniques. In particular, the ¹H NMR spectra of ester **1a**(PF₆⁻) and amide **1b**(PF₆⁻) derivatives, recorded in [D₆]acetone, show the presence of the guanidinium NH protons at 7.30/7.14 ppm for the ester and 7.19/7.13 ppm for the amide analogue, chemical shifts that are typical for guanidinium hexafluorophosphate salts.¹⁶ In addition, signals, which correspond to the TTF hydrogens ($\delta = 7.76/6.69$ ppm for **1a** and $\delta = 7.36/6.66$ ppm for **1b**), are also discernible. The ester or amide junctions were mainly confirmed by the existence of two discrete methylene signals at 67.6 and 46.0 ppm, respectively, in the ¹³C NMR spectra.

With respect to phenyl-C₆₀ (**2a,b**) and biphenyl-C₆₀ derivatives (**3a,b**), inspection of the ¹H NMR spectra (see Figure 1a)

disclose evidence for the pyrrolidine protons, that is, a doublet at ca. 5.1 and 4.1 ppm (CH₂, $J \approx 9.4$ Hz; geminal hydrogens) and a singlet at ca. 5.1 ppm (CH). Similar to **1a** and **1b**, the link between the fullerene and guanidinium fragments was established by the presence of the corresponding signals ($\delta = 65.5$ ppm for both esters **2a** and **3a**; $\delta = 43.5$ ppm for both amides **2b** and **3b**) in the ¹³C NMR spectra.

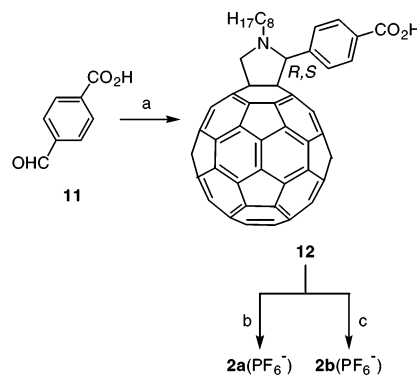
Donor–acceptor dyads **1a•5**, **1b•5**, **1a•6**, and **1b•6** (Chart 2), in which the electron donor (TTF) is directly attached to the guanidinium scaffold and the electron acceptor (phenyl-C₆₀ or biphenyl-C₆₀) is connected to the carboxylate, were prepared by single liquid–liquid extraction. In particular, an aqueous phase of the sodium carboxylates **5**(Na⁺) or **6**(Na⁺) was brought in contact with a dichloromethane solution of the guanidinium hexafluorophosphate salts **1a**(PF₆⁻) and **1b**(PF₆⁻) (see Experimental Section in the Supporting Information for details).

Chart 2. Structures of Hydrogen Bonded C₆₀•TTF DyadsScheme 1. Synthesis of TTF Derivatives **1a,b**(PF₆⁻)^a

^a (a) CH₂Cl₂/2 M aq KOH (×2); then 0.1 M aq NH₄PF₆ (×2), 100%. (b) **10**, *N,N*-diisopropylethylamine (DIPEA), CH₂Cl₂, room temperature, 12 h; then CH₂Cl₂/0.1 M aq NH₄PF₆ (×2), 49%. (c) *N*-Methylmorpholine (NMM), Ms₂O, THF, room temperature, 1 h; then CH₂Cl₂/0.1 M aq NH₄PF₆ (×2), 96%. (d) 30% NH₃, MeOH, room temperature, 30 min, 100%. (e) **10**, DIPEA, CH₂Cl₂, room temperature, 12 h; then CH₂Cl₂/2 M aq KOH (×2) and 0.1 M aq NH₄PF₆ (×2), 72%.

Analogously, acceptor–donor dyads **2a•4**, **2b•4**, **3a•4**, and **3b•4**, with the donor subunit attached to the carboxylate, were prepared by single liquid–liquid extraction of an aqueous solution of lithium TTF-carboxylate **4**(Li⁺)¹⁹ with dichloromethane solutions of the guanidinium salts [**2a**(PF₆⁻), **2b**(PF₆⁻), **3a**(PF₆⁻), and **3b**(PF₆⁻)].

It is worth mentioning that the formation of compounds **2a,b** and **3a,b**, as well as their corresponding supramolecular dyads, should lead to the expected diastereomeric mixture provided that a new stereogenic center is generated in the pyrrolidine

Scheme 2. Synthesis of Phenyl-C₆₀ Derivatives **2a,b**(PF₆⁻)^a

^a (a) C₆₀, *N*-octylglycine, *o*-dichlorobenzene (ODCB), reflux, 16 h, 52%. (b) PyBOP, DIPEA, **7**(Cl⁻), CH₂Cl₂, 80 °C, 3 days; then CH₂Cl₂/2 M aq KOH (×1) and 0.1 M aq NH₄PF₆ (×2), 58%. (c) PyBOP, DIPEA, **9**, CH₂Cl₂, room temperature, 12 h; then CH₂Cl₂/2 M aq KOH (×2) and 0.1 M aq NH₄PF₆ (×2), 73%.

ring. However, even after registering the ¹H NMR spectra of these compounds at high resolution (500 MHz), we were not able to distinguish these diastereomers. The large distance between the pyrrolidine ring and the guanidinium group could account for this experimental finding.

In all the dyads, significant downfield shifts (ca. 4 ppm in CDCl₃) were observed for the guanidinium NH protons (see, for example, Figure 1b), which is consistent with the existence of a strong DD–AA hydrogen bonding arrangement in the new guanidinium-carboxylate ion pair formed.¹⁴

(19) Garín, J.; Orduna, J.; Uriel, S.; Moore, A. J.; Bryce, M. R.; Wegener, S.; Yufit, D. S.; Howard, J. A. K. *Synthesis* **1994**, 489–493.

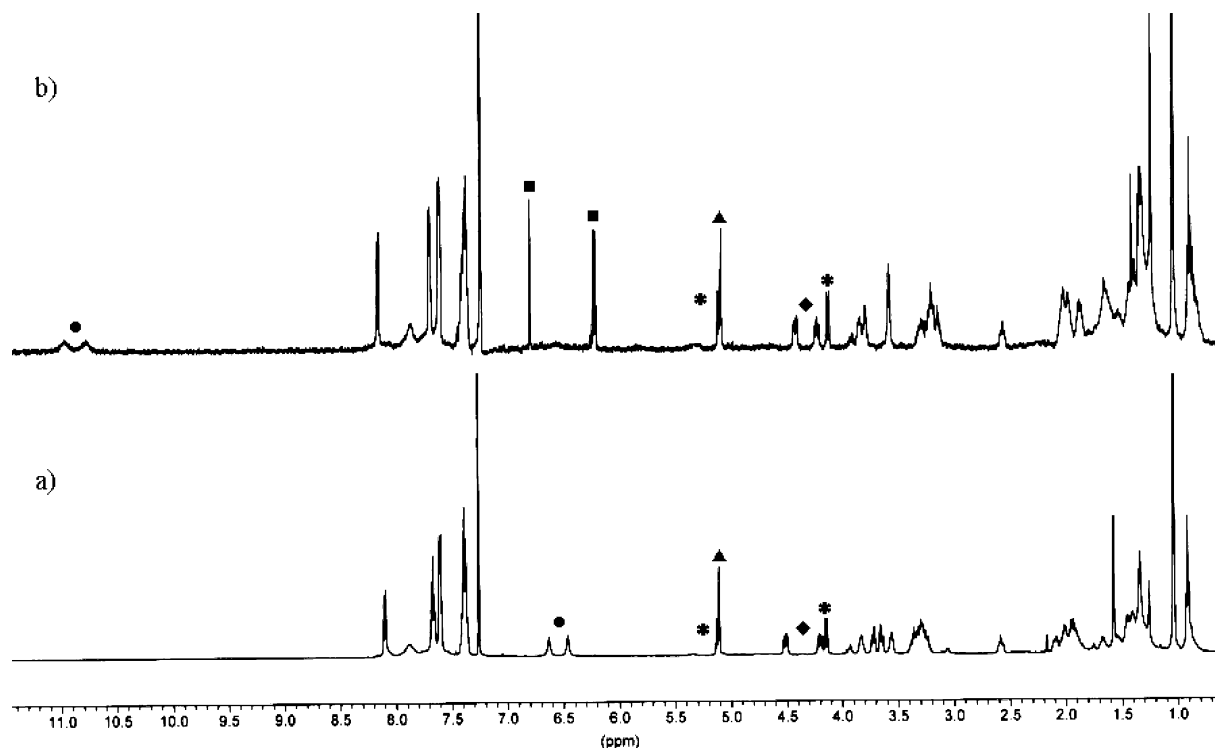
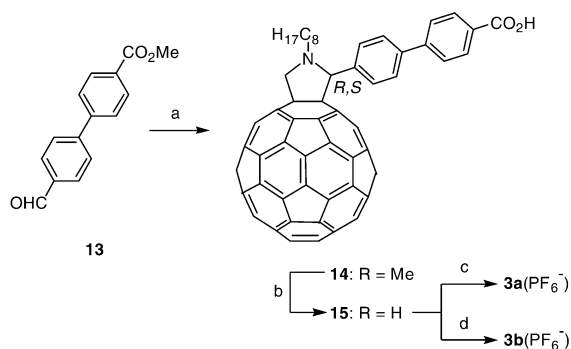


Figure 1. ^1H NMR spectra (500 MHz, CDCl_3) of compound **3a**(PF_6^-) (a) and dyad **3a•4** (b) at room temperature: (●) guanidinium NH^+ s; (■) CH TTF; (▲) CH pyrrolidine; (*) CH_2 pyrrolidine; (◆) CH_2O .

Scheme 3. Synthesis of Biphenyl- C_{60} Derivatives **3a,b**(PF_6^-)^a



^a (a) C_{60} , *N*-octylglycine, ODCB, reflux, 16 h, 51%. (b) HCl, AcOH, ODCB, reflux, 72 h, 65%. (c) PyBOP, DIPEA, **7**(Cl^-), CH_2Cl_2 , 80 °C, 3 days; then $\text{CH}_2\text{Cl}_2/2$ M aq KOH ($\times 1$) and 0.1 M aq NH_4PF_6 ($\times 2$), 67%. (d) PyBOP, DIPEA, **9**, CH_2Cl_2 , room temperature, 12 h; then $\text{CH}_2\text{Cl}_2/2$ M aq KOH ($\times 2$) and 0.1 M aq NH_4PF_6 ($\times 2$), 72%.

Electrochemistry. The redox properties of **1a,b**, **2a,b**, and **3a,b** were measured at room temperature by cyclic voltammetry experiments. We selected a 4:1 *o*-dichlorobenzene/acetonitrile solvent mixture to ensure solubilization of all the fullerene derivatives. The data are collected in Table 1 along with those of the parent TTF and C_{60} moieties, which serve as references.

TTF derivatives **1a,b**, that is, those bearing guanidinium cations, show the presence of two reversible oxidation waves, corresponding to the formation of the radical cation and dication species. These waves are anodically shifted in comparison with the parent TTF, which can be accounted for by the electronic effect of the electron-withdrawing ester and amide carbonyl groups attached to the 1,3-dithiole ring of the TTF moiety. The values determined for the first oxidation potential in **1a,b** reveal the stronger deactivation of the ester group, relative to what is

Table 1. Redox Potentials of New TTF and C_{60} Derivatives

compd ^a	E_{red}^1	E_{red}^2	E_{red}^3	E_{red}^4	$E_{1,\text{ox}}^{1/2}$	$E_{2,\text{ox}}^{1/2}$
1a					0.55	0.99
1b					0.51	0.94
2a	-0.58	-0.97	-1.52	-1.95		
2b	-0.60	-0.98	-1.52	-1.98		
3a	-0.59	-0.99	-1.52	-1.94		
3b	-0.60	-0.99	-1.52	-1.97		
C₆₀	-0.54	-0.94	-1.43	-1.91		
TTF					0.44	0.81

^a Experimental conditions: V vs Ag/Ag^+ ; ODCB/MeCN (4:1) as solvent; GCE as working electrode; $\text{Bu}_4\text{N}^+\text{ClO}_4^-$ (0.1 M) as supporting electrolyte; scan rate, 100 mV/s.

noted for the amide group, thus slightly decreasing the electron donor ability of the TTF unit.

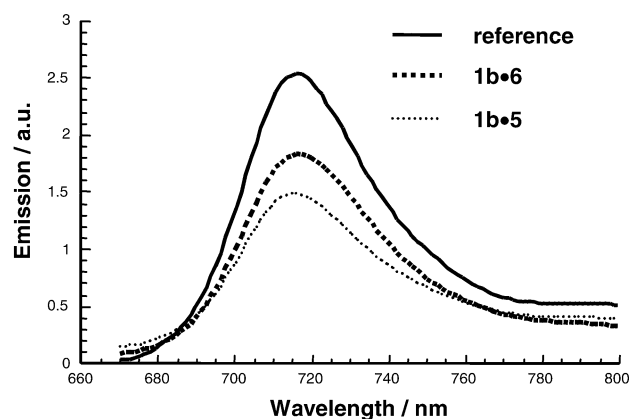
[60]Fullerene derivatives, on the other hand, which are linked to the guanidinium cations through either an ester (**2a**, **3a**) or amide group (**2b**, **3b**) show four quasireversible reduction waves. These reduction waves are cathodically shifted in comparison with the parent C_{60} molecule, measured under the same experimental conditions. Earlier, this electrochemical shift, which is characteristic for most 1,2-dihydrofullerenes, has been rationalized by the saturation of a C_{60} double bond and consequently raising the LUMO energy of the C_{60} derivative.²⁰

Interestingly, the fullerene centered reduction potential peaks appear at nearly identical values. This observation prompts to a lack of electronic communication between the guanidinium, ester or amide group, with C_{60} in the ground state. A similar trend evolves when comparing the phenyl- and biphenyl-based ensembles, which exhibit practically the same reduction potential values (Table 1).

(20) Echegoyen, L.; Echegoyen, L. E. *Acc. Chem. Res.* **1998**, *31*, 593–601.

Table 2. Photophysical Features of Hydrogen Bonded C₆₀•TTF Dyads

	toluene		chloroform		dichloromethane	
	fluorescence quantum yield	fluorescence lifetime (ns)	fluorescence quantum yield	fluorescence lifetime (ns)	fluorescence quantum yield	fluorescence lifetime (ns)
1a•5	3.6×10^{-4}	1.05	2.8×10^{-4}	0.86	2.7×10^{-4}	0.82
1b•5	3.4×10^{-4}	1.05	2.8×10^{-4}	0.83	2.7×10^{-4}	0.80
1a•6	4.2×10^{-4}	1.25	3.3×10^{-4}	1.06	3.3×10^{-4}	1.09
1b•6	4.2×10^{-4}	1.26	3.2×10^{-4}	1.08	3.2×10^{-4}	1.10
2a•4	4.2×10^{-4}	1.19			3.6×10^{-4}	1.02
2b•4	3.9×10^{-4}	1.13			3.4×10^{-4}	0.97
3a•4	4.2×10^{-4}	1.22			3.0×10^{-4}	1.01
3b•4	4.0×10^{-4}	1.24			3.1×10^{-4}	1.06

**Figure 2.** Room-temperature fluorescence spectra of a *N*-methylfulleropyrrolidine reference, dyad **1b•6**, and dyad **1b•5** in toluene solutions. Excitation wavelength is 360 nm.

Steady-State and Time-Resolved Fluorescence Studies. We started the steady-state fluorescence experiments with dyads (**1a•5**, **1b•5**, **1a•6**, **1b•6**, **2a•4**, **2b•4**, **3a•4**, and **3b•4**, Chart 2) by probing solvents which support the well-directed hydrogen bond motif, such as toluene, chloroform, and dichloromethane. Benefits of this solvent variation are the control over the free energy gap for photoinduced charge-transfer processes: In the more polar solvents, a better solvation of charged entities, such as fullerene radical anions and the TTF radical cations, prevails and, subsequently, lowers the energy of the radical ion pairs relative to that of the singlet ground state.

Notably, the TTF electron donor features much weaker absorptions in the visible region than the fullerene core which leads, upon photoexcitation in the 300–400 nm range, to the exclusive fullerene singlet excited-state population (i.e., <95%). All details about the photophysical parameters are summarized in Table 2. The most important observation is that the room-temperature fullerene fluorescence, with its characteristic maximum at 715 nm in toluene, is in C₆₀•TTF dyads (for example, 3.4×10^{-4} for **1b•5**) quenched relative to that of *N*-methylfulleropyrrolidine (6.0×10^{-4}), which was used as a reference. This trend can also be seen in Figure 2. For a given solution, the fluorescence intensity is known to be proportional to the intensity of the exciting light and the molar extinction coefficient. Since these parameters were kept constant, it is conceivable to attribute the decrease in fluorescence intensities to reductive quenching of the fullerene excited singlet state by the TTF moiety via electron transfer.

Earlier reports on intramolecular electron transfer in donor–bridge–acceptor dyads demonstrated the dependence of the rate of electron transfer upon the solvent dielectric constant.²¹

Accordingly, the more polar solvents amplify the fullerene fluorescence quenching (from 3.4×10^{-4} in toluene to 2.7×10^{-4} in dichloromethane for dyad **1b•5**, Table 2).

In addition, the flexible nature of the spacer between TTF and C₆₀ allows a high degree of conformational freedom. Thus, two contrasting scenarios, that is, a through-bond or a more plausible through-space supported electron transfer, might be accountable for the photoreactivity of the C₆₀•TTF dyads. To shed light onto the mechanism in question and differentiate between them, we probed several spacers, since their chemical nature and composition help to modulate the electronic coupling. In the case of simple ester and amide linkages, both spacers place donor and acceptor in approximately the same spatial separation. However, we found no significant differences between esters and amides, 4.2×10^{-4} for both **1a•6** and **1b•6**, and the fullerene deactivation remains unaffected regardless of the solvent. We conclude, from this trend, that a through-space mechanism might be operative. This scenario appears credible in light of a simple molecular modeling, which suggests that donor and acceptor are placed in close proximity to each other.²²

In the second set of dyads, we compared the impact of biphenyl and phenyl spacers on the photoreactivity of the C₆₀•TTF dyads: Using the rigid biphenyl separation instead of phenyl leads to a small but appreciable impact on the fullerene singlet excited-state deactivation. More precisely, a 20% reactivation of the fullerene fluorescence from 3.4×10^{-4} to 4.2×10^{-4} (**1b•5** vs **1b•6**, Table 2 and Figure 2) is seen. This again speaks against a through-bond electron transfer but should be considered in support of a through-space electron-transfer scenario. In fact, in case of a through-bond electron transfer, implementation of four additional bonds into the hydrocarbon bridge should have affected the electron-transfer rate by 2 orders of magnitude (i.e., decrease in rate of nearly 1 order of magnitude *per* introduction of two bonds into the hydrocarbon bridge).²³ The observed rates and yields, however, are in contrast to the increment of bonds in the spacer. Although the fluorescence patterns of the different C₆₀•TTF dyads are nearly

(21) For example, see: Guldi, D. M.; Maggini, M.; Scorrano, G.; Prato, M. *J. Am. Chem. Soc.* **1997**, *119*, 974–980.

(22) Due to the high flexibility of each component, an accurate estimation of the minimum distance between TTF and C₆₀ in each dyad is difficult. The following minimal distances between the centers of the fullerene and the outer TTF ring in ester or amide derivatives were evaluated from the *in vacuo* optimized structures: 6.55 Å for dyads **1a•5** and **2a•4**; 7.84 Å for dyad **3a•4**; and 9.30 Å for dyad **1a•6**.

(23) (a) Oevering, H.; Paddon-Row, M. N.; Heppener, M.; Oliver, A. M.; Cotsaris, E.; Verhoeven, J. W.; Hush, N. S. *J. Am. Chem. Soc.* **1987**, *109*, 3258–3269. (b) Oevering, H.; Verhoeven, J. W.; Paddon-Row, M. N.; Warman, J. M. *Tetrahedron* **1989**, *45*, 4751–4766. (c) Kroon, J.; Verhoeven, J. W.; Paddon-Row, M. N.; Oliver, A. M. *Angew. Chem., Int. Ed. Engl.* **1991**, *30*, 1358–1361. (d) Paddon-Row, M. N. *Acc. Chem. Res.* **1994**, *27*, 18–25. (e) Shephard, M. J.; Paddon-Row, M. N. *Aust. J. Chem.* **1996**, *49*, 395–403.

identical, it should be noted that, parallel to the fluorescence reactivation, the associated maxima shows a bathochromic shift from 715 to 718 nm, as compared to that determined for the *N*-methylfulleropyrrolidine reference. This suggests alteration of the through-space communication and confirms the creation of through-space electronic interactions between the two chromophores in the dyads.

An independent test on the validity of the fluorescence quantum yields involved fluorescence lifetime measurements, by recording the kinetic time profiles of the 715 or 718 nm fluorescence maxima upon 337 nm fullerene excitation. For the *N*-methylfulleropyrrolidine reference, we determined a lifetime of 1.5 ns in toluene and dichloromethane, which is notably longer than the corresponding values in all of the C_{60} •TTF dyads. As can be seen from a closer inspection of Table 2, the values determined for the different dyads and/or in the different solvents agree quantitatively and qualitatively with the quantum yields.

When comparing the fluorescence data for the dyads in which donors and acceptors are placed in a converse fashion, for example, for shorter contact distances, compare **1a•5** with **2a•4** (or **1b•5** with **2b•4**), we note that in all solvents employed the interactions were stronger in the **1** series (TTF at the guanidinium) than in the **2** series (C_{60} at the guanidinium), whereas, in the biphenyl series, in which the spacer keeps both components wide apart, for example, **1a•6** versus **3a•4**, no significant differences were observed.

Therefore, hydrogen bonds emerge as an effective means to hold the electron donor (TTF) and the electron acceptor (C_{60}) in spatially predetermined positions. To manipulate the organization principle, a protic solvent, such as hexafluoro-2-propanol (HFIP), which interferes with the existing $-NH\cdots O-C-$ network, was combined with dichloromethane. The addition of HFIP resulted in a quantitative recovery of the fullerene fluorescence; that is, the quantum yields (6.0×10^{-4}) are now comparable to that of the *N*-methylfulleropyrrolidine reference. This result confirms the complete interruption of the integrative hydrogen bond network and the C_{60} •TTF complex dissociation into both independent fragments (i.e., C_{60} and TTF). Similarly, the fluorescence lifetime of 1.4 ns in the HFIP–dichloromethane mixtures becomes almost identical with that seen for the *N*-methylfulleropyrrolidine reference under identical experimental conditions (Figure S2).

Transient Absorption Spectroscopy. To confirm the fluorescence behavior we employed transient absorption spectroscopic technique with the *N*-methylfulleropyrrolidine reference and the different C_{60} •TTF dyads (**1a•5**, **1b•5**, **1a•6**, **1b•6**, **2a•4**, **2b•4**, **3a•4**, and **3b•4**). This allows, besides establishing intra- and intermolecular dynamics, such as charge-recombination rates, identifying the product evolving from the initial fullerene deactivation, suggested by the fluorescence experiments.

As far as the fulleropyrrolidines are concerned, they exhibit on the nano-/microsecond time scale transient transitions ascribable exclusively to the long-lived (i.e., 20 μ s) triplet excited state. These are sets of maxima at 360 and 700 nm; see the Supporting Information. Figure 3 illustrates the 700–1100 nm region, recorded for a dichloromethane solution of *N*-methylfulleropyrrolidine and **1b•5**. For the dyad, the differential absorption changes are fundamentally different from what is seen for the fulleropyrrolidine. Clearly, a new feature at 1000

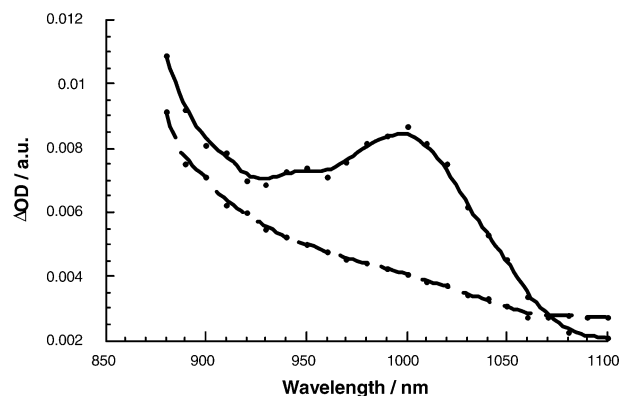


Figure 3. Differential absorption changes recorded 50 ns after a 337 nm laser excitation of *N*-methylfulleropyrrolidine (dashed spectrum) and dyad **1b•5** (solid spectrum) in deoxygenated dichloromethane.

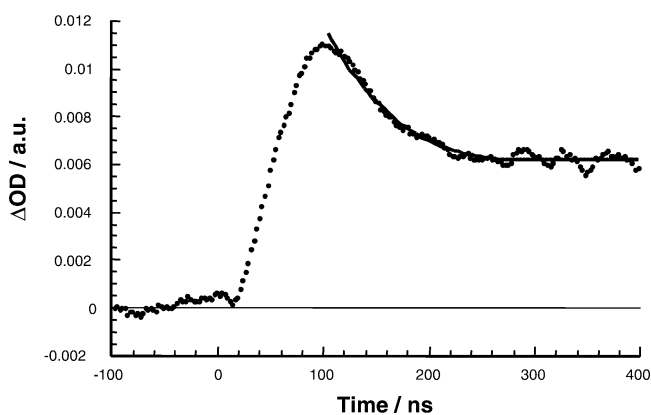


Figure 4. Time-absorption profile of the C_{60} radical anion absorption decay (i.e., at 1000 nm) as recorded upon a 337 nm laser excitation of dyad **1b•5** in deoxygenated dichloromethane.

nm is discernible, which resembles the characteristic fullerene radical anion marker. In addition, we found the 450 nm transition of the TTF radical cation. This spectroscopic evidence confirms the metastable electron transfer, evolving from the initially excited fullerene core.

Fitting the decay dynamics of $C_{60}^{\bullet-}$ and $TTF^{\bullet+}$ to a first-order rate law, we determined lifetimes of 115 ns (dyad **1a•5**, not shown) and 124 ns (dyad **1b•5**, Figure 4) for the radical ion pairs $C_{60}^{\bullet-}$ • $TTF^{\bullet+}$ in dichloromethane, which corresponds to charge-recombination rates of $(8.4 \pm 0.3) \times 10^6 \text{ s}^{-1}$. More drastic is the impact of the distance dependence, that is, phenyl versus biphenyl spacer. In the latter systems, the charge-recombination process is considerably decelerated. For example, a rate of $1.0 \times 10^6 \text{ s}^{-1}$, measured for the **1a•6** dyad, results from a smaller electronic coupling between donor and acceptor.²⁴

Addition of the hydrogen bond breaking solvent HFIP changes the fullerene reactivity. Most importantly, right after the laser pulse, no evidence for the $C_{60}^{\bullet-}$ • $TTF^{\bullet+}$ radical pair formation was seen. Instead, the sole species formed is the fullerene triplet in 95% efficiency, similar to what is shown for the *N*-methylfulleropyrrolidine reference in Figure 3. Due to the presence of the non-hydrogen bonded electron donor, the fullerene triplet excited state is, however, subject to an

(24) In line with the moderate electron-transfer efficiency, also the product of the fullerene intersystem crossing, the triplet excited state with its characteristic 700 nm fingerprint is discernible. In chloroform or dichloromethane, the triplet quantum yields are, however, on the order of 30%.

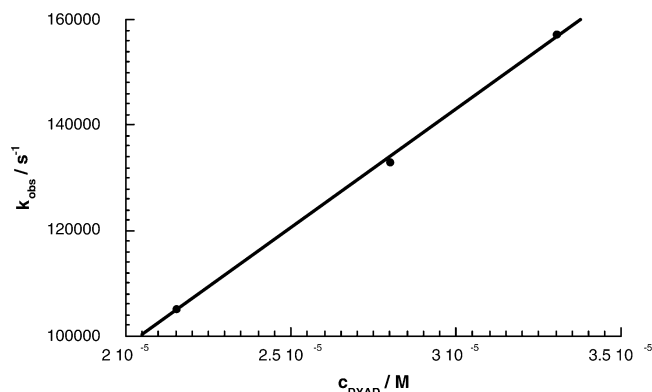


Figure 5. Plot of k_{obs} versus $C_{1\mathbf{b}\cdot\mathbf{5}}$ at various concentrations in deoxygenated HFIP–dichloromethane (1:1).

intermolecular electron-transfer quenching. From a concentration dependence (i.e., $(0.2\text{--}5.0) \times 10^{-5}$ M for dyad **1b.5**), we derived a rate constant of $4.5 \times 10^9 \text{ M}^{-1} \text{ s}^{-1}$ in the HFIP–dichloromethane mixture (Figure 5). This value is in good agreement with intermolecular electron-transfer rates measured for fullerene triplets with diverse electron donors, including TTF itself.²³

Conclusions

In retrospect, we demonstrated that hydrogen bonding motifs confer outstanding benefits for constructing photo- and electroactive donor–acceptor models as novel artificial photosynthetic systems and possible photovoltaic applications.

In the current work, we reported on the design, synthesis, and physicochemical study of new supramolecular fullerene architectures. These architectures are built on highly directional and selective hydrogen bonding as a biomimetic organization principle. We started with synthesizing a series of novel TTF and C_{60} precursors that carry either a complementary guanidinium or carboxylate entity. A complementary array of hydrogen bonds, donor–donor–acceptor–acceptor (DD–AA), opens the way to incorporate both moieties into well-ordered donor–acceptor arrays: **1a.5**, **1b.5**, **1a.6**, **1b.6**, **2a.4**, **2b.4**, **3a.4**, and **3b.4**. Varying the nature and composition of the spacer connecting TTF and C_{60} , by using different functional

groups (i.e., ester versus amide) and length spacer (i.e., phenyl versus biphenyl), allowed the construction of topologically different ensembles. This provided meaningful incentives to differentiate between through-bond and through-space supported electron-transfer interactions.

Steady-state and time-resolved emission studies show a clear trend toward fluorescence quenching in the $C_{60}\bullet$ TTF dyads whose efficiency depends predominantly on the solvent polarity. Electron transfer, as the cause of fluorescence quenching, was confirmed independently by transient absorption spectroscopy. In particular, the rapid formation of the characteristic fullerene radical anion (1000 nm) and TTF radical cation (450 nm) transitions clearly attests $C_{60}^{\bullet-}\bullet$ TTF $^{\bullet+}$. Charge recombination rates in the $C_{60}\bullet$ TTF ensembles are typically around 10^6 s^{-1} depending on electronic coupling between donor and acceptor. Owing to the complexity of the network that connects C_{60} with TTF in our dyads and the flexible nature of the spacer, through-space electron-transfer interactions are operative to create the charge separated $C_{60}^{\bullet-}\bullet$ TTF $^{\bullet+}$ state, although this photophysical process is not very efficient. Addition of the hydrogen bonding-breaking solvent HFIP, on the other hand, results in a change of the photochemical reactivity, in which no evidence for forming an intramolecular CS state is observed. Alternatively, an intermolecular electron-transfer process takes place.

Acknowledgment. We are indebted to MCyT of Spain (Projects BQU-2002-00855 and PB98-0088) and the Office of Basic Energy Sciences of the U.S. Department of Energy (Contribution No. NDRL-4490 from the Notre Dame Radiation Laboratory) for financial support. A grant from Comunidad Autónoma de Madrid (to M.S.) is also gratefully acknowledged. The authors would like to acknowledge Dr. Pilar Prados and Dr. Michiel Van Gool for helpful discussions and suggestions.

Supporting Information Available: General experimental procedures for the synthesis of guanidinium salts (**1–3**) and C_{60} -based carboxylic acids (**12**, **15**) as well as supramolecular dyads. This material is available free of charge via the Internet at <http://pubs.acs.org>.

JA036358N